1 **An infection and pathogenesis mouse model of SARS-CoV-2-related pangolin**

2 **coronavirus GX_P2V(short_3UTR)**

3

4 Lai Wei[1,#], Shuiqing Liu[1,#], Shanshan Lu[1,#], Shengdong Luo[2], Xiaoping An[1], Huahao

5 Fan[1], Weiwei Chen[2], Erguang Li[3,*], Yigang Tong[1,*], Lihua Song[1,*]

6

7 [1] Beijing Advanced Innovation Center for Soft Matter Science and Engineering,

8 College of Life Science and Technology, Beijing University of Chemical Technology,

9 Beijing, China. [2]Research Center for Clinical Medicine, The Fifth Medical Center of

10 PLA General Hospital, Beijing, China. [3]State Key Laboratory of Pharmaceutical

11 Biotechnology, Medical School, Nanjing University, China

12 [#]Contributed equally.

13 [*]email: erguang@nju.edu.cn; tong.yigang@gmail.com; songlihua@gmail.com

14

15 **ABSTRACT**

16 SARS-CoV-2-related pangolin coronavirus GX_P2V(short_3UTR) is highly

17 attenuated, but can cause mortality in a specifically designed human ACE2-transgenic

18 mouse model, making it an invaluable surrogate model for evaluating the efficacy of

19 drugs and vaccines against SARS-CoV-2.

20 **KEYWORDS:** pangolin coronavirus, human ACE2-transgenic mouse, SARS-CoV-2,

21 COVID-19

22

23

24 **INTRODUCTION**

25    Two SARS-CoV-2-related pangolin coronaviruses, GD/2019 and GX/2017, were

26 identified prior to the COVID-19 outbreak (1, 2). The respective isolates, termed

27 pCoV-GD01 and GX_P2V, were cultured in 2020 and 2017, respectively (2, 3). The

28 infectivity and pathogenicity of these isolates have been studied (4-6). The

29 pCoV-GD01 isolate, which has higher homology with SARS-CoV-2, can infect and

30 cause disease in both golden hamsters and hACE2 mice (4). In contrast, GX_P2V was

31 found to be highly attenuated in previously tested animals like golden hamsters,

32 BALB/c mice and two types of human ACE2-transgenic (hACE2) mouse (5, 6). We

33 previously reported that the early passaged GX_P2V isolate was actually a cell

34 culture-adapted mutant, named GX_P2V(short_3UTR), which possesses a

35 104-nucleotide deletion at the 3'-UTR (6). In this study, we analyzed its adaptive

36 mutation in cell culture, and assessed its pathogenicity in a unique CAG-hACE2

37 mouse model. We found that GX_P2V(short_3UTR) can infect hACE2 mice, with

38 high viral loads detected in both lung and brain tissues, which are correlated with the

39 strong expression of hACE2 in these tissues. This infection resulted in 100%

40 mortality in the hACE2 mice. We surmise that the cause of death may be linked to the

41 occurrence of late brain infection.

42 **RESULTS**

43    We first analyzed the adaptive mutations of the GX_P2V(short_3UTR) mutant in

44 cell cultures by random cloning and sequencing. The passaged mutant was cloned

45 through two successive plaque assays. Eight viral clones were chosen for

46 next-generation sequencing (National Genomics Data Center of China, GSA:

47 CRA014225). These clones, when compared with the genome of the original mutant

48 (6), all shared four identical mutations: ORF1ab_D6889G, S_T730I, S_K807N, and

49 E_A22D (Supporting Information, Table S1). Clone 7, named as GX_P2V C7, was

50 randomly selected for the evaluation of viral pathogenicity in hACE2 mice (Figure

51 1A). The hACE2 mouse model expressing human ACE2 under control of the CAG

52 promoter was developed using random integration technology by Beijing SpePharm

53 Biotechnology Company.

54　　　Next, we assessed whether GX_P2V C7 could cause disease in hACE2 mice by

55 monitoring daily weight and clinical symptoms. A total of four 6 to 8-week-old

56 hACE2 mice were intranasally infected with a dosage of $5\times10^5$ plaque-forming units

57 (pfu) of the virus. Four mice inoculated with inactivated virus and four mock-infected

58 mice were used as controls. Surprisingly, all the mice that were infected with the live

59 virus succumbed to the infection within 7-8 days post-inoculation, rendering a

60 mortality rate of 100% (Figure 1B). The mice began to exhibit a decrease in body

61 weight starting from day 5 post-infection, reaching a 10% decrease from the initial

62 weight by day 6 (Figure 1C). By the seventh day following infection, the mice

63 displayed symptoms such as piloerection, hunched posture, and sluggish movements,

64 and their eyes turned white. The criteria for clinical scoring of the mice and the daily

65 clinical scores post-infection with GX_P2V C7 are provided in the Supporting

66 Information, Figure S1.

67　　　We then evaluated the tissue tropism of GX_P2V C7 in hACE2 mice. Using the

68    infection method described above, eight hACE2 mice were infected, eight mice were

69    inoculated with inactivated virus, and another eight mock-infected mice were used as

70    controls. The organs of four randomly selected mice in each group were dissected on

71    days 3 and 6 post-infection for quantitative analysis of viral RNA and titer. We

72    detected significant amounts of viral RNA in the brain, lung, turbinate, eye, and

73    trachea of the GX_P2V C7 infected mice (Figure 1D), whereas no or a low amount of

74    viral RNA was detected in other organs such as the heart, liver, spleen, kidneys,

75    tongue, stomach, and intestines. Specifically, in lung samples, we detected high viral

76    RNA loads on days 3 and 6 post-infection, with no significant difference between

77    these two time points ($\sim$ 6.3 versus $\sim$ 5.8 $\mathrm{Log}_{10}$[copies/mg]). In brain samples, on day

78    3 post-infection, viral RNA was detected in all four infected mice, with an average

79    value of 5.4 $\mathrm{Log}_{10}$[copies/mg]. Notably, by day 6 post-infection, we detected

80    exceptionally high viral RNA loads ($\sim$ 8.5 $\mathrm{Log}_{10}$[copies/mg]) in the brain samples

81    from all four infected mice (Figure 1D). On days 3 and 6 post-infection, the viral

82    RNA loads in the turbinate were similar, approximately 4.1 and 3.9 $\mathrm{Log}_{10}$[copies/mg],

83    respectively. The viral RNA loads in the trachea and eyes of the mice surpassed the

84    limit of detection only on day 6 post-infection, with values of 2.6 and 3.8

85    $\mathrm{Log}_{10}$[copies/mg], respectively. Regarding the infectious viral titers, lung tissues at

86    day 3 post-infection had a value of $\sim$ 1.8 $\mathrm{Log}_{10}$[pfu/mg], which decreased to $\sim$ 0.5

87    $\mathrm{Log}_{10}$[pfu/mg] by day 6. Importantly, the highest infectious titers were detected in the

88    brain on day 6, which was significantly greater than that on day 3 ($\sim$ 0.9 vs $\sim$ 4.8

89    $\mathrm{Log}_{10}$[pfu/mg]) (Figure 1E). Additionally, there were no significant differences in the

90    infectious titers in the turbinate between day 3 ($\sim$ 0.9 $\text{Log}_{10}$[pfu/mg]) and day 6 ($\sim$ 1.2

91    $\text{Log}_{10}$[pfu/mg]) (Figure 1E). By day 6, approximately 2.0 $\text{Log}_{10}$[pfu/mg] was detected

92    in the eyes of two mice. Neither inactivated GX_P2V C7 nor mock infection caused

93    death or any clinical symptoms in the mice (Figure 1B-C and Supporting Information,

94    Figure S2). In summary, in the mice infected with live virus, the viral load in the

95    lungs significantly decreased by day 6; both the viral RNA loads and viral titers in the

96    brain samples were relatively low on day 3, but substantially increased by day 6. This

97    finding suggested that severe brain infection during the later stages of infection may

98    be the key cause of death in these mice.

99          To determine the mechanisms underlying GX_P2V C7-induced death in hACE2

100    mice, we examined the pathological changes, presence of viral antigens, and cytokine

101    profiles in the lung and brain tissues of the mice on days 3 and 6 post-infection

102    (Figure 1F-G, and Supporting Information, Figure S3 and S4). On both days,

103    compared to those of control mice, the lungs of infected mice showed no significant

104    pathological alterations, with only minor inflammatory responses due to slight

105    granulocyte infiltration (Figure 1F). On day 3 post-infection, shrunken neurons were

106    visible in the cerebral cortex of the mice. By day 6, in addition to the shrunken

107    neurons, there was focal lymphocytic infiltration around the blood vessels, although

108    no conspicuous inflammatory reaction was observed (Figure 1G). Upon staining for

109    viral nucleocapsid protein via immunohistochemistry, viral antigens were detected in

110    both the lungs and brains on days 3 and 6 post-infection, with extensive viral antigens

111    notably present in the brain on day 6 (Figure 1F-G). These findings align with the

112    viral RNA load assessments in the lung and brain tissues (Figure 1D). We also

113    performed a Luminex cytokine assay to detect 31 cytokines/chemokines in the lung

114    and brain tissues of the mice (Supporting Information, Figure S3 and S4). Consistent

115    with the pathological findings, there were slight increases or decreases in the levels of

116    many cytokines/chemokines in lung and brain tissues compared to those in control

117    tissues, but the levels of key inflammatory factors, such as IFN-γ, IL-6, IL-1β, and

118    TNF-α, did not significantly change. In brief, these analyses revealed that GX_P2V

119    C7 infection in hACE2 mice did not lead to severe inflammatory reactions, a finding

120    that aligns with previous reports by Zhengli Shi's group using GX_P2V infection in

121    two different hACE2 mouse models (5), as well as our own findings in the golden

122    hamster model (6).

123    **DISCUSSION**

124        To the best of our knowledge, this is the first report to analyze the cell-adapted

125    mutations of pangolin coronavirus GX_P2V, and to show it can cause mortality in

126    hACE2 mice. Our findings are evidently inconsistent with those of Zhengli Shi *et al*.

127    (5), who tested the virulence of GX_P2V in two different hACE2 mouse models. It is

128    very likely that the high pathogenicity of GX_P2V C7 in our hACE2 mice is due to

129    the strong expression of hACE2 in the mouse brain. Under normal circumstances,

130    both human and mouse brains exhibit low expression of ACE2 (6, 7). Furthermore,

131    while the company has not yet published a paper detailing the construction and

132    characterization of this hACE2 mouse model, we are notified that these hACE2 mice

133    have abnormal physiology, as indicated by relatively reduced serum triglyceride,

134   cholesterol, and lipase levels, compared to those of wild-type C57BL/6J mice. Thus,

135   the outcomes from the mouse infections in this study have no correlation with human

136   infections, and do not alter the fundamental nature of GX_P2V(short_3UTR) as being

137   highly attenuated.

138       Currently, there is an urgent need for the development of broadly protective

139   vaccines against pan-SARS-CoV-2, yet the emergence of the next SARS-CoV-2

140   variant is unpredictable. The pangolin coronavirus GX_P2V(short_3UTR), which

141   shares a certain degree of homology with SARS-CoV-2, may be valuable in assessing

142   the effectiveness of broad-spectrum COVID-19 vaccine candidates against unknown

143   future variants. Moreover, our lethal mouse infection model presents no obvious

144   inflammatory responses in the main affected organs, the lungs and brain, thereby

145   providing an alternative model to evaluate antiviral drugs' efficacy in inhibiting viral

146   replication *in vivo*. In summary, our study provides a unique perspective on the

147   pathogenicity of GX_P2V and offers an invaluable model for assessing the efficacy of

148   drugs and vaccines against SARS-CoV-2.

149

150   **REFERENCES**

151   1.  Liu P, Chen W, Chen JP. Viral Metagenomics Revealed Sendai Virus and

152   Coronavirus Infection of Malayan Pangolins (Manis javanica). Viruses. 2019 Oct

153   24;11(11).

154   2.  Lam TT, Jia N, Zhang YW, Shum MH, Jiang JF, Zhu HC, et al. Identifying

155   SARS-CoV-2-related coronaviruses in Malayan pangolins. Nature. 2020

Jul;583(7815):282-5.

3. Xiao K, Zhai J, Feng Y, Zhou N, Zhang X, Zou JJ, et al. Isolation of SARS-CoV-2-related coronavirus from Malayan pangolins. Nature. 2020 Jul;583(7815):286-9.

4. Huang XY, Chen Q, Sun MX, Zhou HY, Ye Q, Chen W, et al. A pangolin-origin SARS-CoV-2-related coronavirus: infectivity, pathogenicity, and cross-protection by preexisting immunity. Cell Discov. 2023 Jun 17;9(1):59.

5. Liu MQ, Lin HF, Li J, Chen Y, Luo Y, Zhang W, et al. A SARS-CoV-2-Related Virus from Malayan Pangolin Causes Lung Infection without Severe Disease in Human ACE2-Transgenic Mice. J Virol. 2023 Feb 28;97(2):e0171922.

6. Lu S, Luo S, Liu C, Li M, An X, Li M, et al. Induction of significant neutralizing antibodies against SARS-CoV-2 by a highly attenuated pangolin coronavirus variant with a 104nt deletion at the 3'-UTR. Emerg Microbes Infect. 2023 Dec;12(1):2151383.

7. Natalia Alenina, Michael Bader. ACE2 in Brain Physiology and Pathophysiology: Evidence from Transgenic Animal Models. Neurochem Res. 2019 Jun;44(6):1323-1329. doi: 10.1007/s11064-018-2679-4.

8. Meng-Yuan Li, Lin Li, Yue Zhang, Xiao-Sheng Wang. Expression of the SARS-CoV-2 cell receptor gene ACE2 in a wide variety of human tissues. Infect Dis Poverty. 2020 Apr 28;9(1):45. doi: 10.1186/s40249-020-00662-x.

**ACKNOWLEDGEMENTS**

178     32161143027), National Key R&D Program of China (2021YFC2301804) and

179     Biosafety Special Program (No. 19SWAQ 13).

180     **ETHICS STATEMENT**

181     All animals involved in this study were housed and cared for in an AAALAC

182     (Association for Assessment and Accreditation of Laboratory Animal Care) accredited

183     facilities. The procedure for animal experiments (IACUC-2019-0027) was approved

184     by the Institutional Animal Care and Use Committee of the Fifth Medical Center,

185     General Hospital of the Chinese People's Liberation Army, and complied with IACUC

186     standards.

187     **AUTHOR CONTRIBUTIONS**

188     L.Song conceived and designed the study and wrote the manuscript. L.W., S.Liu,

189     S.Lu., and S.Luo. performed the experiments and analyzed the data. X.A., H.F., W.C.,

190     E.L. and Y.T. analyzed the data and edited the manuscript. L.W. and L.Song wrote the

191     manuscript and all the authors approved the manuscript.

192     **CONFLICT OF INTERESTS**

193     The authors declare no competing interests.

194     **SUPPORTING INFORMATION**

195     Additional Supporting Information for this article can be found online at

196     **DATA AVAILABILITY**

197     All the data supporting the findings of this study are available within the article and

198     the Supporting Information, or from the corresponding author upon reasonable

199     request.

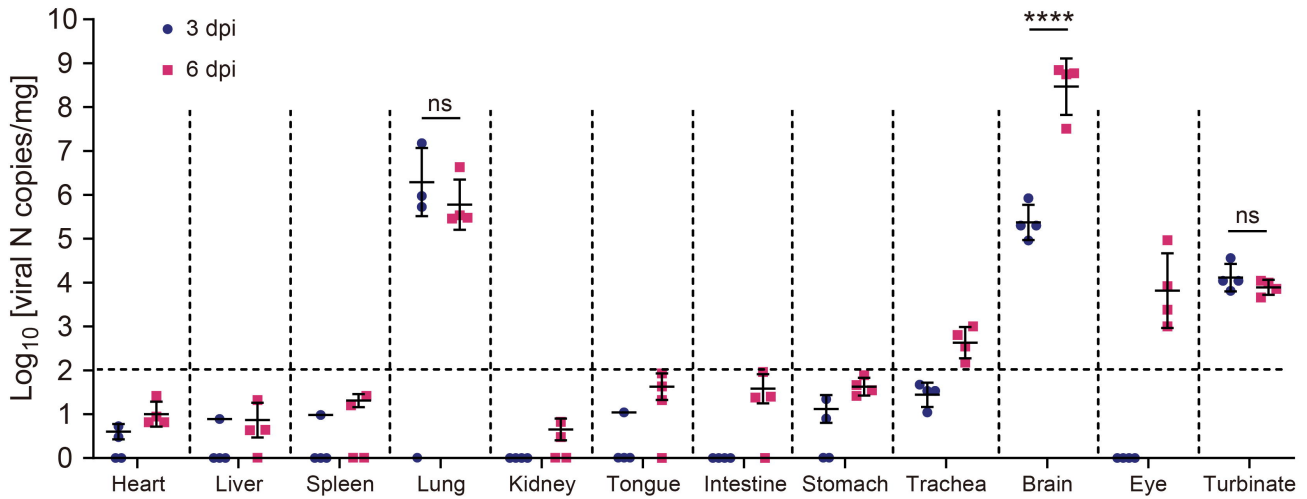200 **ORCID**

201    Lihua Song, https://orcid.org/0000-0002-7299-5719
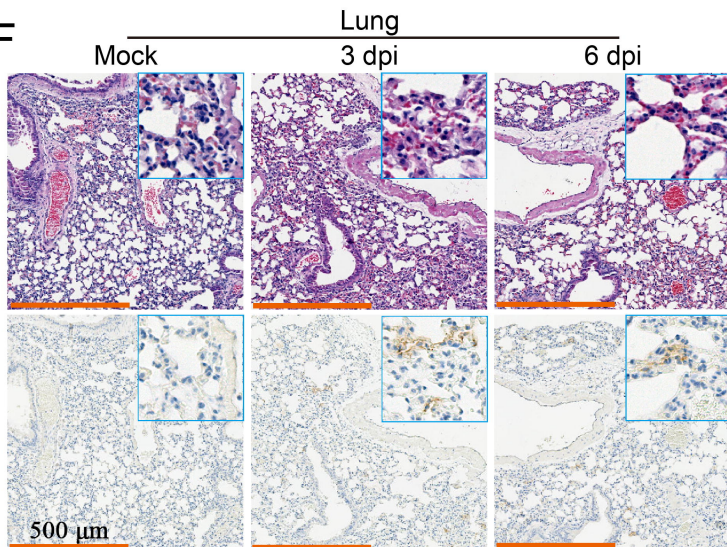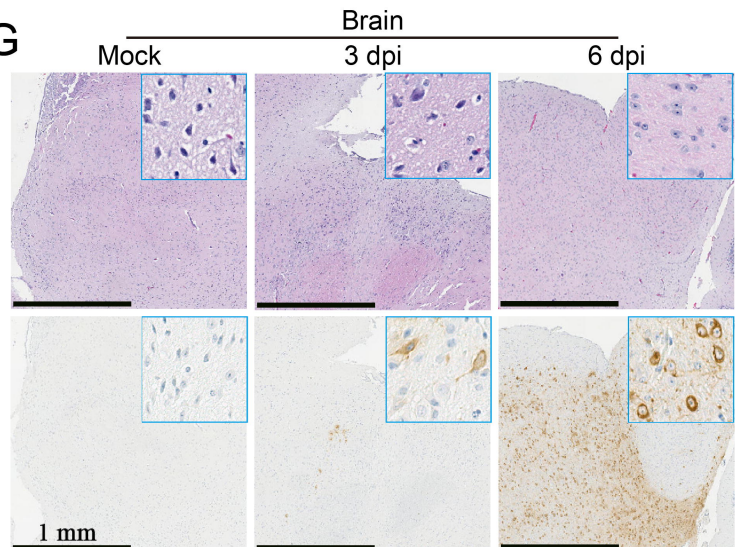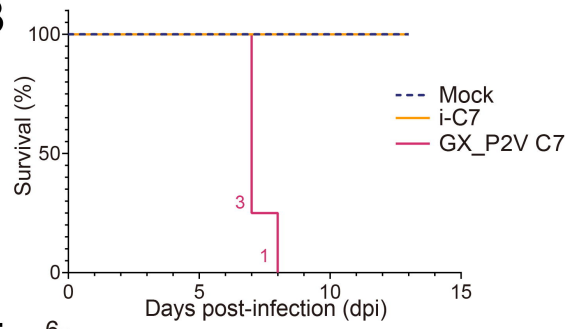
Pdf by:
https://www.pro-memoria.info

202  **Figure 1: Characterization of a lethal infection model in human**

203  **ACE2-transgenic mice caused by the attenuated SARS-CoV-2-related pangolin**

204  **coronavirus GX_P2V C7. A** Mutations in GX_P2V C7 compared to the

205  GX_P2V(short_3UTR) isolate (NCBI accession number: MW532698). The four

206  identical mutations are shown in bold. **B** Survival of hACE2 transgenic mice

207  following intranasal infection with GX_P2V C7 ($n = 4$), inactivated GX_P2V C7

208  (i-C7, $n = 4$), and mock infection ($n = 4$). The number of deceased mice on each

209  specific day is annotated on the left of the survival curve. **C** Percentage of initial

210  weight of hACE2 transgenic mice after intranasal infection with GX_P2V C7 ($n = 4$),

211  i-C7 ($n = 4$), and mock infection ($n = 4$). The statistical significance of the differences

212  between mock-infected ($n = 4$, blue dots) and GX_P2V C7-infected ($n = 4$, red dots)

213  or i-C7-infected mice ($n = 4$, orange dots) at 6 or 7 dpi are shown. The error bars

214  represent the means ± SDs. **D** Quantification of GX_P2V N gene copies in heart, liver,

215  spleen, lung, kidney, tongue, intestine, stomach, trachea, brain, eye, and turbinate

216  homogenates at 3- and 6-day post-infection (dpi) ($n = 4$ per group). The limit of

217  detection (LOD) for viral RNA loads in the original samples was $Log_{10}[10^2$

218  copies/mg]. The error bars represent the means of $Log_{10}[copies/mg]$ ± SDs. The

219  significances of the comparisons in the lung, brain, and turbinate are shown. **E**

220  Infectious viral titers in lung, brain, eye, and turbinate homogenates were measured

221  by plaque forming assay at 3 and 6 dpi ($n = 4$ per group). The statistical significance

222  of the differences in the lung, brain, and turbinate are shown. The error bars represent

223  means of $Log_{10}[pfu/mL]$ ± SDs. **F, G** Hematoxylin and eosin (H&E) staining and

224     immunohistochemical (IHC) staining with an anti–SARS-CoV-2 N-specific antibody

225     (SARS-CoV-2) revealed viral antigen–positive cells (brown) in the lung (**F**) and brain

226     (**G**), as shown at high magnification in the inset. Scale bars, 500 μm (**F**) and 1 mm

227     (**G**), respectively. *$P < 0.05$, **$P < 0.01$, ***$P < 0.001$, ****$P < 0.0001$, $P > 0.05$, not

228     significant (ns); two-way ANOVA followed by Sidak's multiple comparison test.

**A**

| Mutation | Codon change | Substitution | CDS Location |
|---|---|---|---|
| 1807 A to G | GGA to GGG | | ORF1ab |
| 6501 C to U | ACA to AUA | T to I | ORF1ab |
| 19694 C to U | ACA to AUA | T to I | ORF1ab |
| **20930 A to G** | **GAU to GGU** | **D to G** | **ORF1ab** |
| **23727 C to U** | **ACU to AUU** | **T to I** | **S** |
| **23959 A to C** | **AAA to AAC** | **K to N** | **S** |
| **26274 C to A** | **GCU to GAU** | **A to D** | **E** |
| 29227 C to U | UAC to UAU | | N |

**B**

Survival (%)

Days post-infection (dpi)

Mock
i-C7
GX_P2V C7

**C**

Percentage of initial weight (%)

Days post-infection (dpi)

Mock
i-C7
GX_P2V C7

ns    ns
****  ****

**E**

Log₁₀ [viral PFU/mg]

3 dpi
6 dpi

Lung    Brain    Eye    Turbinate

**    ****    ns

**D**

Log₁₀ [viral N copies/mg]

3 dpi
6 dpi

Heart  Liver  Spleen  Lung  Kidney  Tongue  Intestine  Stomach  Trachea  Brain  Eye  Turbinate

ns    ****    ns

**F**

Lung

Mock    3 dpi    6 dpi

500 μm

**G**

Brain

Mock    3 dpi    6 dpi

1 mm